Journal of Ethnopharmacology 268 (2021): 113668

DOI: https://doi.org/10.1016/j.jep.2020.113668

Graphical Abstract

Anti-inflammatory, pro-proliferative and antimicrobial potential of the compounds isolated from *Daemonorops draco* (Willd.) Blume

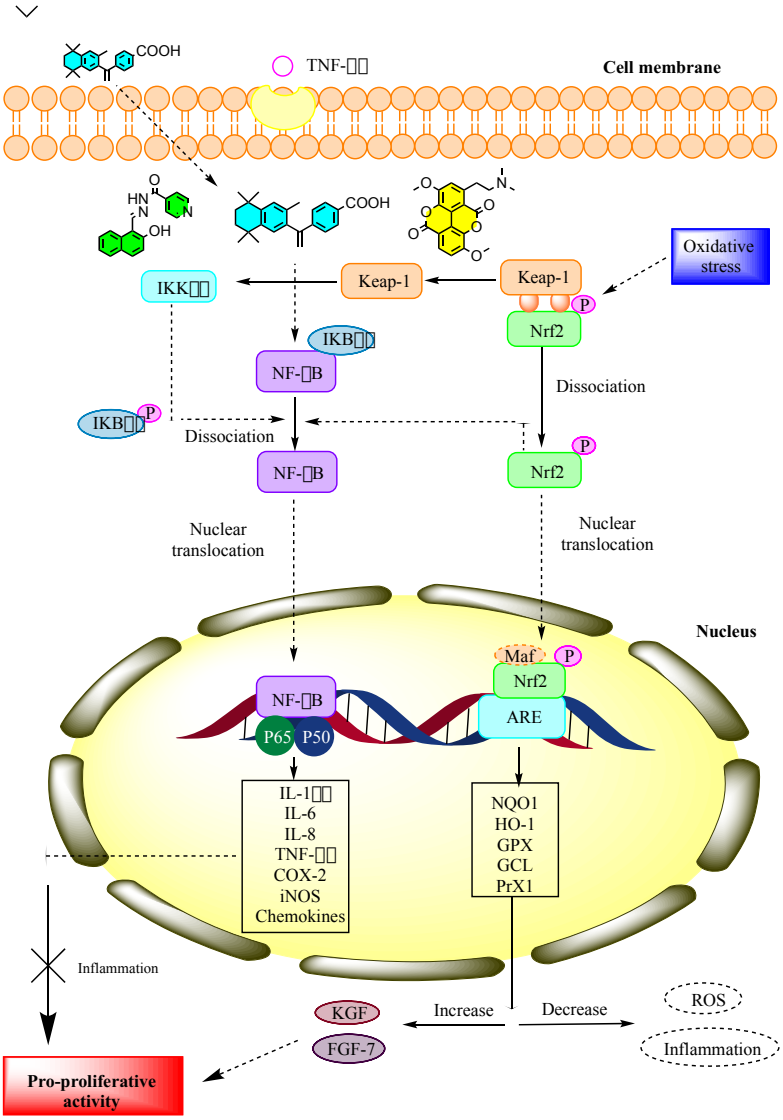

Anti-inflammatory, pro-proliferative and antimicrobial potential of the compounds isolated from *Daemonorops draco* (Willd.) Blume

Apaza Ticona L[a,b*], Rumbero Sánchez A[a], Sánchez Sánchez-Corral J[a], Iglesias Moreno P[b], Ortega Domenech M[c]

[a] *Department of Organic Chemistry, Faculty of Sciences, Universidad Autónoma de Madrid. Cantoblanco, 28049 Madrid, Spain.*

[b] *Department of Pharmacology, Pharmacognosy and Botany, Faculty of Pharmacy, Universidad Complutense de Madrid. Plza. Ramón y Cajal s/n, 28040 Madrid, Spain.*

[c] *Dr. Goya Análisis, SL, Alcalá de Henares, 28805, Madrid, Spain*

*Corresponding author:

Luis Apaza Ticona. Department of Organic Chemistry, Faculty of Sciences, Universidad Autónoma de Madrid. Cantoblanco, 28049 Madrid, Spain

E-mail: luis.apaza@uam.es; lnapaza@ucm.es

Phone: +34 91 497 4715

Abstract

Ethno-pharmacological relevance: Daemonorops draco (*D. draco*) commonly known as "Dragon´s blood" is one of the most used plants by Momok, Anak Dalam and Talang Mamak tribes from Indonesia as a remedy for wound healing.

Aim of the study: This study aimed to identify the extract, fractions and compounds responsible for the anti-inflammatory and pro-proliferative activities of the *D. draco* resin. Additionally, the antimicrobial activity against two bacteria and one yeast species was analysed.

Materials and methods: Bio-guided isolation of compounds with anti-inflammatory, pro-proliferative and antimicrobial activities from the *D. draco* resin was carried out by measuring: the inhibition of NF-κB and activation of Nrf2 in THP-1, HaCaT, NIH-3T3 cells; cell proliferation in NIH-3T3 and HaCaT cells; and the antimicrobial effect on *E. coli*, *S. aureus* and *C. albicans.*

Results: Guided isolation by bioassay gave rise to the isolation and characterisation by nuclear magnetic resonance and mass spectrometry of three compounds: **1** (Bexarotene), **2** (Taspine) and **3** (2-hydroxy-1-naphthaldehyde isonicotinoyl hydrazone). All compounds showed NF-κB inhibitory activity with IC_{50} values of 0.10-0.13, 0.22-0.24 and 3.75-4.78 μM, respectively, while the positive control, Celastrol, had an IC_{50} of 7.96 μM. Likewise, all compounds showed an activating effect of Nrf2 with EC_{50} values of 5.34-5.43, 163.20-169.20 and 300.82-315.56 *n*M, respectively, while the positive control, CDDO-Me, had an EC_{50} of 0.11 *n*M. In addition, concerning the pro-proliferative activity, compound **1** (IC_{50}=8.62-8.71 *n*M) showed a capacity of 100%, compound **2** (IC_{50}=166-171 *n*M) showed a capacity of 75 %, and compound **3** (IC_{50}=469-486 *n*M) showed a capacity of 65%, while FSB 10% (positive control) had a pro-proliferative activity of 100% in the NIH3T3 cell lines (fibroblasts) and HaCaT (keratinocytes).

Finally, all the compounds showed antimicrobial activity with MIC values of 0.12-0.16, 0.31-0.39 and 3.96-3.99 μM, respectively, in *S. aureus*, *E. coli* and *C. albicans* strains, while the positive control, Ofloxacin, had a MIC of 27.65 μM.

Conclusion: This study managed to isolate, for the first time, three compounds (Bexarotene, Taspine and 2-hydroxy-1-naphthaldehyde isonicotinoyl hydrazone) from the resin of *D. draco*, with anti-inflammatory, and pro-proliferative as well as antimicrobial activities.

Keywords: *Daemonorops*; Dragon´s blood; wound healing; anti-inflammatory; pro-proliferative; antimicrobial

Abbreviatures:

AcOEt:	Ethyl Acetate
ARE:	Antioxidant Responsive Element
ATCC:	American Type Culture Collection
BOD:	Bio-Oxygen Demand
CC_{50}:	Cytotoxic Concentration 50%
CDDO-Me:	2-Cyano-3,12-dioxo-oleana-1,9-(11)-dien-28-oic acid methyl ester
CFU:	Colony-Forming Unit
$CI_{95\%}$:	Confidence Interval 95%
DCM:	Dichloromethane
DH2O:	Distilled Water
DMEM:	Dulbecco's Modified Eagle Medium
DMSO:	Dimethyl Sulfoxide
DTT:	Dithiothreitol
EGF:	Epidermal Growth Factor
ELISA:	Enzyme-Linked Immunosorbent Assay
EtOH:	Ethanol
FBS:	Fetal Bovine Serum
HEX:	*n*-Hexane
HO-1:	Heme Oxygenase 1
IC_{50}:	Inhibitory Concentration 50%
LDH:	Lactate Dehydrogenase
MeOH:	Methanol
MHB:	Mueller-Hinton broth
MIC:	Minimum Inhibitory Concentration

NBM: Nutrient Broth Medium

NF-κB: Nuclear Factor Kappa-Light-Chain-Enhancer of Activated B Cells

Nrf2: Nuclear Factor Erythroid 2-related Factor 2

PBS: Phosphate-Buffered Saline

QTOF: Quadrupole Time-of-Flight

RLUs: Relative Luminescence Units

ROS: Reactive Oxygen Species

TLC: Thin Layer Chromatography

TMS: Tetramethylsilane

TNF-α: Tumour Necrosis Factor-α

TGF-β: Transforming Growth Factor-β

ZI: Zone of Inhibition

1. Introduction

Skin is one of the most important organs for the human being since it constitutes the first defence barrier. For this reason, it is continuously exposed to all kinds of external agents that trigger a series of inflammatory reactions (Proksch, 2018; Kabashima *et al*., 2019). When an injury (wound, abrasion, burn, cut) occurs on the skin, a healing process starts, aiming to repair and regenerate the damaged tissues (Gonzalez *et al*., 2016; Zhao *et al*., 2016). This process can be divided in four stages: coagulation, inflammation, proliferation and maturation (Ashrafi *et al*., 2016; Sami *et al*., 2019).

Regarding the inflammation stage, there are reports on the role of pro-inflammatory cytokines released by macrophages in the positive regulation of inflammatory reactions and in the process of the pathological pain (Cavaillon, 2018). In this sense, the pro-proliferative activity is accelerated through adequate temporal downward regulation of pro-inflammatory cytokine levels (Opal & DePalo, 2000). Within cytokines, the NF-κB (Nuclear Factor Kappa-Light-Chain-Enhancer of Activated B Cells) cytokine has a crucial role in the pathogenesis of several inflammatory diseases (Lawrence, 2009).

Additionally, several works suggest the importance of Nrf2 (Nuclear Factor Erythroid 2-related Factor 2) during processes of cell proliferation and differentiation, as well as tissue repairing, regulating protein expression (Ambrozova *et al*., 2017; Hiebert & Werner, 2019). Keratinocytes of the hyperproliferative epithelium of skin wounds were shown to strongly express Nrf2, but expression of this gene was also described in cells of the granulation tissue (Ambrozova *et al*., 2017). Nrf2 has also been shown to be activated after tissue damage and synergised with other transcription factors such as NF-κB, enabling the pro-proliferative process (Eichenfield *et al*., 2016).

Finally, infection is one of the significant causes of delayed wound healing (Gottrup *et al*., 2013); therefore, infection control should be carefully considered for curing wounds. To

116 control infection, wounds should be treated with aseptic techniques and appropriate
117 antimicrobial agents (Vermeulen *et al*., 2010). During the infection, pro-inflammatory
118 cytokines (e.g. TNF-α, NF-κB) are important regulators of host responses to microbial
119 challenges (Ziltener *et al*., 2016). These cytokines amplify and coordinate pro-inflammatory
120 signals that lead to the expression of effector molecules, thus inducing the modulation of the
121 diverse aspects of the innate immunity against infection (Hop *et al*., 2017).

122 In this context, the pro-proliferative process can be enabled by natural products with
123 medicinal properties (Fazil & Nikhat, 2020). Different studies have focused on the pro-
124 proliferative properties of natural products with anti-inflammatory, antimicrobial and pro-
125 collagen synthesis properties (Agyare *et al*., 2019). These medicinal properties can be
126 attributed to the bioactive phytochemical constituents of alkaloids, essential oils, flavonoids,
127 tannins, terpenoids, saponins and phenolic compounds (Georgescu *et al*., 2016).

128 Among medicinal plants with pro-proliferative, anti-inflammatory and antimicrobial
129 activities, the plant species called "Dragon´s blood" has been studied for its traditional use in
130 different cultures (Egypt, China, India, South America) (Gupta *et al*., 2007). Among the several
131 species identified as “Dragon´s blood” (species of the Croton, Dracaena, Pterocarpus and
132 Daemonorops genera), we will analyse in this work the *Daemonorops draco* species.

133 *Daemonorops draco* (Willd) Blume, belonging to the Arecaceae family, is a native
134 species from Indonesia, which has been traditionally used by the Momok, Anak Dalam and
135 Talang Mamak tribes as a remedy for treating wounds because of its anti-haemorrhagic, anti-
136 inflammatory and healing properties (Sulasmi, 2012a; 2012b). The *D. draco* species has been
137 reported to contain triterpenes, flavans, chalcones (Nasini & Piozzi, 1981), diterpene acids
138 (Piozzi *et al*., 1974) and biflavonoids (Merlini & Nasini, 1976). 57 compounds have been
139 isolated and characterised from the resin of *D. draco*, with 14 out of the 57 compounds showing
140 pharmacological activities. The chloroform, ethyl acetate and methanol extracts have been

reported as having antimicrobial (Wahyuni *et al*., 2018), antioxidant (Purwanti *et al*., 2019) and anti-inflammatory (Kuo *et al*., 2017) activities.

This article aims to provide a scientific basis for the traditional use of *Daemonorops draco* as a remedy for wound treatment. In this sense, a bio-guided phytochemical study was carried out to identify those *D. draco* compounds with anti-inflammatory potential (inhibition of NF-κB production and Nrf2 activation) and pro-proliferative activity in NIH-3T3 and HaCaT cells; and with antimicrobial activity in three microbial strains (*Candida albicans*, *Escherichia coli* and *Staphylococcus aureus*).

2. Material and methods

2.1. Plant Material

Daemonorops draco was collected from the Baxian Mountain National Nature Reserve, located at the southern slope of the Yanshan mountain chain, northeast of Jixian County, Tianjin, China (40°11'56.4"N and 117°33'60.0"E), in December 2018, at an altitude of 1046.8 m. Botanical identification was confirmed by the Tianjin Natural History Museum, and a voucher specimen was deposited (TJC 0729). The fruits were left to dry for three days at a temperature of 25±5°C, to avoid the compounds from suffering some type of decomposition and/or chemical modification. Subsequently, the crushing and pulverisation was carried out using a knife and hammer mill (Greiffenberger Antriebstechnik GmbH Marktredwitz model), to promote the powdery detachment of the fruit resin. Finally, the resin was sieved to obtain a homogeneous powder with a particle size of 2 mm.

166 *2.2. General experimental procedures*

167 First grade organic solvents were used for isolating the compounds and they were
168 purchased from Sigma-Aldrich. Column chromatography was performed with silica gel (20-
169 45 μm and 40-63 μm, Merck). TLC was performed using Merck Silica gel 60-F_{254} plates.
170 Chromatograms thus obtained were visualised by UV absorbance (254 nm) and through
171 heating a plate stained with a 5% phosphomolybdic acid solution in EtOH 95% (Ethanol 95%)
172 followed by heat application.

173 NMR experiments were performed on the Bruker Advance DRX 300 and 500
174 spectrometers operating at 300 MHz, 500 MHz (^{1}H) or 76 MHz, and 126 MHz (^{13}C) with TMS
175 (Tetramethylsilane) as the internal standard. The deuterated solvents were $CDCl_3$-d_1 and
176 MeOD-d_4. Spectra were calibrated by assignment of the residual solvent peak to δ_H 7.26, δ_H
177 3.31 and δ_C 77.16, δ_C 49.00, for $CDCl_3$ and MeOD, respectively. The complete assignment of
178 protons and carbons was done by analysing the correlated ^{1}H-^{1}H COSY, ^{1}H-^{13}C HSQC and
179 ^{1}H-^{13}C HMBC spectra.

180 Mass spectra were performed on a mass spectrometer with a QTOF (Quadrupole Time-
181 of-Flight) hybrid model QSTAR *pulsar i analyser* from the commercial company AB Sciex.
182 The samples were analysed using the electrospray ionisation technique in positive and negative
183 ion detection mode. They were introduced into the mass spectrometer by direct infusion at a
184 flow of 10 μL/min, using a syringe pump.

185

186 *2.3. Extraction and isolation*

187 350 g of the dry powder of the fruits of *D. draco* were extracted by repeated maceration
188 (3 times/24 h/25ºC) with 500 mL of different solvents, increasing the polarity: HEX (*n*-Hexane),
189 DCM (Dichloromethane), MeOH (Methanol) and DH2O (Distilled Water). Subsequently, the
190 extracts were filtered, and the respective solvents were removed by vacuum rotary evaporation

191 at room temperature (25ºC). As a result, four extracts of 8 g, 25 g, 19 g and 6 g, respectively,
192 were obtained.

193 Dichloromethane extract (20 g) was selected as the most active one and was fractionated
194 using a chromatographic column (4x40 cm) with Si-60 Silica gel (40-63 μm, Merck) as a
195 stationary phase and a DCM/MeOH gradient (9.5:0.5→0:1) as eluent. A total of eleven fractions
196 (F1-F11) were obtained: F1 (0.169 g), F2 (0.038 g), F3 (0.054 g), F4 (0.084 g), F5 (0.112 g), F6
197 (0.074 g), F7 (0.075 g), F8 (0.039 g), F9 (0.117 g), F10 (0.233 g) and F11 (0.123 g).

198 Subsequently, based on the biological activity data, a second separation of F2 was carried
199 out by using a chromatographic column (4x40 cm) with Si-60 Silica gel (40-63 μm, Merck) as a
200 stationary phase and a HEX/AcOEt (Ethyl Acetate) gradient (19.5:0.5→0:1). A total of eight
201 fractions (I-VIII) were obtained: F2.I (2.3 mg), F2.II (3.1 mg), F2.III (4 mg), F2.IV (1.1 mg),
202 F2.V (3.5 mg), F2.VI (4.3 mg), F2.VII (2.5 mg), and the F2.VIII (6.7 mg) which was the
203 compound RDDDCM-F2.VIII (**1**).

204 On the other hand, a liquid-liquid extraction was carried out to obtain an extract rich in
205 alkaloids, using the methodology of Tsacheva *et al*. (2004). 3.80 g of dry powder were left
206 stirring for 30 minutes with 100 mL of DCM and 50 mL of 6% ammonia. It was then extracted
207 repeatedly with DCM (3x100 mL). The organic fractions were combined and concentrated by
208 rotary evaporation to remove the solvent.

209 The alkaloid-rich dichloromethane extract (1.8 g) showed a pharmacological activity
210 similar to the dichloromethane extract, so it was subjected to column chromatography (3x25
211 cm) on silica gel (20-40 μm) at medium pressure in HEX (125 mL), dioxane and MeOH (250
212 mL) in a gradient of increasing polarity. The fractions obtained were grouped according to the
213 results of the chromatographic analysis by TLC (Thin Layer Chromatography), obtaining three
214 fractions (F1´-F3´). Further purification of the active fractions (F1´ and F2´) on silica gel
215 microcolumns yielded the compounds RDDDCM-ALK_F1´ (**2**) and RDDDCM-ALK_F2´ (**3**).

2.4. Cell culture reagents and drugs

Three cell lines were used in this study: NIH-3T3 (Mouse embryo fibroblast, CRL-1658), HaCaT (Human skin keratinocyte, PCS-200-011) and THP-1 (Human peripheral blood monocyte, TIB-202) cells were used as a negative control to evaluate the cytotoxicity of the samples. All cell lines were obtained from the ATCC (American Type Culture Collection). Cells were cultured in specific media according to ATCC recommendations. The incubation condition for all cells was at an atmosphere of 95% air and 5% CO_2 at 37°C.

DMEM (Dulbecco's Modified Eagle Medium, Sigma-Aldrich, St. Louis, MO, USA), FBS (Fetal Bovine Serum, Summit Biotechnology; Ft. Collins, CO) and PBS (Phosphate-Buffered Saline, SAFC Biosciences, Inc. Andover-Hampshire, UK) were used as culture mediums. L-glutamine was obtained from Applichem. Penicillin and streptomycin were purchased from Fisher Scientific (Pittsburgh, PA). For cytotoxicity and activity assays the compounds were dissolved in DMSO (Dimethyl Sulfoxide, Merck) at a concentration of 10 mM, while extracts and fractions were dissolved at 20 mg/mL in DMSO.

2.5. Cytotoxicity assay

The samples were determined in a panel of two cell lines (NIH-3T3 and HaCaT) and a control cell line (THP-1) by means of the LDH (Lactate Dehydrogenase) assay at different concentrations (100, 50, 25, 12.5, 6.25, 3.125, 1563, 0.781, 0.391 and 0.95) in μg/mL (extracts and fractions) or μM (compounds). The cells were seeded in 96-well plates at a density of $3x10^3$ cells/well and incubated overnight at 37°C in a humidified atmosphere of 5% CO_2. Subsequently, the cells were treated with the extracts or compounds at different concentrations and using DMSO as a control for 48 h. Actinomycin D (≥95% Sigma-Aldrich, CAS Number 50-76-0) was used as a positive control at a concentration of 7.97 *n*M, showing cell death. After 48 h of treatment with the extracts or compounds, 100 μL of culture supernatants were collected

and incubated in the reaction mixture of the LDH kit (Innoprot Company). After 30 min, the reaction was stopped by the addition of 1 N HCl, and the absorbance at a wavelength of 490 nm was measured using a spectrophotometric ELISA (Enzyme-Linked Immunosorbent Assay plate reader, SpectraMax® i3, Molecular Devices).

2.6. In vitro anti-inflammatory activity

2.6.1. NF-κB inhibition assay

Cells (3×10^3 cells/well) were stably transfected with the KBF-Luc plasmid, which contains three copies of NF-κB binding site (from a major histocompatibility complex promoter), fused to a minimal simian virus 40 promoter driving the luciferase gene. Cells were seeded the day before the assay on 96-well plate. The cells were then treated with samples (extracts, fractions and compounds) at the same concentrations used in the viability assays for 15 min and then they were stimulated with 30 *n*g/mL TNF-α. Celastrol (≥98% Sigma-Aldrich, CAS Number 34157-83-0) was used as a positive control at a concentration of 7.41 μM. After 48 h, the cells were washed twice with PBS and lysed for 15 min in a 50 μL buffer containing 25 mM Tris-phosphate (pH 7.8), 8 mM $MgCl_2$, 1 mM DTT (Dithiothreitol), 1% Triton X-100 and 7% glycerol, at room temperature, using a horizontal shaker. The luciferase activity was measured using a GloMax 96 microplate luminometer (Promega) following the instructions of the luciferase assay kit (Promega, Madison, WI, USA). The RLU (Relative Luminescence Units) was calculated and the results were expressed as percentage of inhibition of NF-κB activity induced by TNF-α (100% activation). The experiments for each concentration of the assay elements were performed in triplicate wells.

266 *2.6.2. Nrf2 activity assay*

267 All cells contained the Nqo1 ARE-Luc reporter plasmid. ARE (Antioxidant Responsive
268 Element) was activated by all members of the CNC family of factors (Nrf1, Nrf2, Nrf3 and
269 p45 NF-E2). The cells were cultivated in 96-well plates at the concentration of $3x10^3$
270 cells/well in a CO_2 incubator at 37ºC. For induction of Nrf2 activation, the cells were treated
271 for 48 h with samples (extracts, fractions and compounds) at the same concentrations used in
272 the viability assays. As a positive control, the cells were treated with CDDO-Me (≥98%
273 Sigma-Aldrich, CAS Number 218600-53-4), used at a concentration of 0.11 *n*M. Then the
274 cells were washed twice in PBS and lysed in 25 mM Tris-phosphate pH 7.8, 8 mM $MgCl_2$, 1
275 mM DTT, 1% Triton X-100 and 7% glycerol during 15 min at room temperature, using a
276 horizontal shaker. The luciferase activity was measured using a GloMax 96 microplate
277 luminometer (Promega), following the instructions of the luciferase assay kit (Promega,
278 Madison, WI, USA). The results obtained from the lysis buffer were subtracted from each
279 experimental value, and the specific transactivation expressed as fold induction over basal
280 levels (untreated cells). The experiments for each concentration of the assay items were done
281 in triplicate wells.

282

283 *2.7. Evaluation parameters of the pro-proliferative activity*

284

285 *2.7.1. Real-time pro-proliferative activity assay*

286 NIH-3T3 and HaCaT cells (3×10^3 cells/well) were seeded in a 96-well Essen
287 ImageLock plate (Essen BioScience) and grown to confluence in a CO_2 humidified incubator
288 in the absence of FBS. As a positive control, the cells were treated with 10% FSB (Summit
289 Biotechnology; Ft. Collins, CO). After 24 h, the scratch was made using the 96-pin
290 WoundMaker (Essen BioScience). Wound images were taken every 3 h for 48 h, and the data

was analysed with the Relative Wound Density integrated metric. This is part of the IncuCyte HD live content cell imaging system (Essen BioScience).

2.8. In-vitro antimicrobial activity

2.8.1. Microorganisms

In the present study, strains of three microorganisms were used: Gram-positive *Staphylococcus aureus* (ATCC 25904); Gram-negative *Escherichia coli* (ATCC 25922D-5) and *Candida albicans* yeast (ATCC 10231). These three microorganisms were chosen because they are predominant opportunistic pathogens in skin infections (Petkovsek *et al*., 2009; Kashem & Kaplan, 2016; Hülpüsch *et al*., 2020).

2.8.2. Agar well diffusion method

For the cultivation of the bacterial strains, NBM (Nutrient Broth Medium) was prepared using 8% nutrient broth in double DH2O and agar-agar. It was subjected to autoclaving at 15 Ibs psi for 30 min/s. Agar plates were prepared by pouring 15 mL of NBM into petri dishes under aseptic condition and kept at room temperature (25ºC) for stabilisation. Bacterial cell cultures were maintained in peptone saline solution by regular sub-culturing and were incubated at 37ºC for 24 h (Apaza *et al*., 2020).

Agar plates were inoculated by streaking 3 times the swab of bacterial strains over the entire sterile agar surface, and rotating the agar plate at 60° for uniform distribution of the inoculum. The plates were dried at room temperature under aseptic condition followed by boring of 9 mm diameter wells. Serial dilutions (100, 50, 25, 12.5, 6.25, 3.12, 1.56, 0.78, 0.39 and 0.19 μg/mL) of the samples (extracts, fractions and compounds) and standard drug Ofloxacin (27.67 μM) were prepared using DMSO as solvent. The samples (100 μL) were

added in wells by using sterile micropipette. The plates were then incubated in a BOD (Bio-Oxygen Demand) incubator at 37ºC for 48 h. The zone of inhibition (ZI) of each bacterial strain was measured in triplicate by using a calibrated digital Vernier caliper.

2.8.3. Broth microdilution method - MIC

MICs (Minimum Inhibitory Concentration) of the extracts, fractions and compounds against the bacterial and yeast strains and samples were determined using the microdilution method in 96 well plates (Cellstar®, Greinerbio-one, Germany) (Apaza *et al*., 2020). The MHB (Mueller-Hinton broth) medium (180 μL) of the bacterial culture and the Sabouraud medium (yeast culture) were used to fill the first experimental well. The other wells were filled with 100 μL of medium. Subsequently, a volume of 20 μL of (extracts, fractions and compounds) was added to the first well. Double fold serial dilution was then carried out across the plate. Overnight batch culture of the microorganisms (10 μL) was used to inoculate each well to achieve an inoculum size of ca. 1×10^6 CFU (Colony-Forming Unit)/mL. The plates were incubated for 48 h at 37ºC. MICs were calculated according to Apaza *et al.* (2020). DMSO at the same tested concentration was used as a negative control, while Ofloxacin (27.67 μM) was used as positive control to assess the accuracy of the MIC method. Each MIC determination was carried out in triplicate.

2.9. Statistical analysis

CC_{50} (Cytotoxic Concentration 50%) and IC_{50} (Inhibitory Concentration 50%) values were determined by non-linear regression. All the experiments were performed in triplicate. One-way ANOVA statistical analysis (Tukey's multiple comparisons test, $p<0.05$; $p<0.001$) was performed to evaluate the significant differences among values. All the analyses were performed using GraphPad Prism, version 8.4.0.

3. Results

3.1. Extraction, isolation and characterisation of compounds

In this report, we only include a detailed characterisation of compounds **1** and **3**, since they have not been previously reported as natural compounds. For compound **2**, only a brief characterisation has been included, because it has been widely described in numerous works as an isolated compound from different plant species (Figure 1).

Figure 1.

3.1.1. Characterisation of compound 1

4-[1-(3,5,5,8,8-Pentamethyl-5,6,7,8-tetrahydro-2-naphthalenyl)-vinyl]-benzoic acid or Bexarotene (**1**) was obtained as a white solid amorphous. Its molecular formula, $C_{24}H_{28}NaO_2$, was confirmed through HRESIMS $[M+Na]^+$ ion at m/z 371.2.

Nineteen signals were distinguished in the ^{13}C NMR spectrum, with seven signals between δ_C: 150-130 ppm corresponding to seven quaternary aromatic carbons. Likewise, between δ_C: 129-126 ppm, three signals correspond to five aromatic carbons (=CH-). The ^1H NMR spectrum showed ten signals differentiable into three systems of signals.

The first system is composed of two doublets of a proton which is coupled to the protons H-α (δ_H: 5.35 ppm, J=1.3 Hz) and H-β (δ_H: 5.83 ppm, J=1.3 Hz) of the vinyl substituent. Through the HSQC spectrum, it was confirmed that the H-α and H-β protons belong to the vinyl carbon (δ_C: 117.33 ppm). Likewise, through the HMBC spectrum, it was confirmed that the signals of the H-α and H-β protons are coupled with the α-vinyl carbon (δ_C: 149.28 ppm) and with the aromatic carbons C-2 (δ_C: 138.06 ppm) and C-1' (δ_C: 146.62 ppm).

Regarding the second benzyl system, it was observed that the protons H-5'/H-3' (δ_H: 8.07 ppm) are coupled with the equivalent protons H-6'/H-2' (δ_H: 7.41 ppm). Furthermore, from the HSQC and HMBC spectra, the H-5'/H-3' protons correspond to the C-5'/C-3' carbons (δ_C: 128.23 ppm). Likewise, the H-5'/H-3' protons are coupled with the C-1' carbons (δ_C: 146.62 ppm), carbonyl (δ_C: 171.10 ppm) and C-4' (δ_C: 130.45 ppm). Finally, the C-6'/C-2' carbons (δ_C: 128.07 ppm) are coupled with the α-vinyl carbon (δ_C: 149.28 ppm).

Through the ^{1}H-^{1}H COSY, HSQC and HMBC spectra, we observed a methyl group in position 3 (δ_C: 20.09 ppm) in the third naphthenic system, with a singlet of three protons (δ_H: 1.95 ppm) which are coupled with the aromatic proton H-4 (δ_H: 7.08 ppm) (Figure 2).

Figure 2.

On the other hand, a methyl was observed in the position 3, which was coupled with the aromatic carbons C-3 (δ_C: 132.86 ppm), C-2 (δ_C: 138.06 ppm) and C-6'/C-2' (δ_C: 128.07 ppm). In addition, it was observed that carbon C-3 couples with the aromatic proton H-1 (δ_H: 7.13 ppm) and with the methyl protons in position 3.

Likewise, it was observed that the aromatic protons H-1 and H-4 are coupled with the C-8/C-5 carbons (δ_C: 35.35-35.37 ppm). A doublet of twelve protons was also observed at δ_H: 1.29 ppm, corresponding to four methoxy groups that are coupled with the C-7/C-6 carbons (δ_C: 34.16-34.06 ppm) and with the C-8/C-5 carbons. Finally, it was observed that the methyl groups at positions 12-15 and the C-6/C-7 carbons correlate with the C-9 (δ_C: 144.58 ppm) and C-10 (δ_C: 142.53 ppm) carbons.

391 *3.1.2. Characterisation of compound 2*

392 1-[2-(Dimethylamino)-ethyl]-3,8-dimethoxychromeno-[5,4,3-cde]-chromene-5,10-
393 dione or Taspine (**2**) was obtained as an amorphous white solid; ^{1}H NMR (300 MHz,
394 $CDCl_3$-d_1) δ_H: 8.13-8.11 (1H, d, H-10), 7.23 (1H, d, H-9), 7.12 (1H, s, H-3), 4.04 (6H, s,
395 2-OCH_3/8-OCH_3), 3.41 (2H, s, H-15'/H-15"), 2.57 (2H, m, H-16'/H-16"), 2.33 (6H, s, 17-
396 CH_3/18-CH_3); ^{13}C NMR (76 MHz, $CDCl_3$-d_1) δ_C: 158.95 (C-12), 157.94 (C-6), 151.38-
397 151.15 (C-2/C-8), 144.15 (C-7), 137.99-136.92 (C-1/C-4), 127.07 (C-10), 119.32 (C-14),
398 118.58 (C-13), 116.82 (C-3), 113.83 (C-11), 111.67 (C-9), 109.32 (C-5), 60.32 (C-16),
399 56.71-56.65 (2-OCH_3/8-OCH_3), 45.18 (C-17/C-18), 32.99 (C-15); $C_{20}H_{19}NO_6$. The
400 spectroscopic data obtained for compound **2** were corroborated with the available literature
401 references (Cheng *et al.*, 2009; Altieri *et al.*, 2013).

402

403 *3.1.3. Characterisation of compound 3*

404 *N*'-[(*E*)-(2-Hydroxy-1-naphthyl)-methylene]-isonicotinohydrazide or 2-hydroxy-1-
405 naphthaldehyde isonicotinoyl hydrazone **(3)** was obtained as an amorphous white solid.
406 Its molecular formula, $C_{17}H_{12}N_3O_2$, was confirmed through HRESIMS $[MH]^-$ ion at m/z
407 290.093.

408 The ^{13}C NMR spectrum showed that the imidolate carbon (C-12) appears at δ_C:
409 160.69 ppm, and the azomethine carbon (C-11) appears at δ_C: 151.34 ppm. The aromatic
410 carbons, corresponding to the naphthenic ring and to isonicotynil ring, appeared between
411 δ_C: 109-160 ppm. The ^{1}H NMR spectrum showed a one-proton singlet at δ_H: 9.58 ppm
412 assigned to the allylic proton C<u>H</u>=N- (H-11). Next, two two-protons multiplets appeared
413 at δ_H: 9.16-9.09 ppm and δ_H: 8.59-8.52 ppm that were assigned to the equivalent protons
414 H-15/H-16 and H-14/H-17 of the isonycotynil ring. A correlation of the C-15/C-16
415 carbons (δ_C: 145.11 ppm) with the C-14/C-17 carbons (δ_C: 126.47 ppm) was observed

through the HSQC spectrum. The correlations between the protons that make up the isonicotinyl ring, and between H-15/H-16 protons and the C-12 carbons (δ_C: 160.69 ppm) and C-13 (δ_C: 149.56 ppm) were observed through the HMBC spectrum.

We did not identify a resonance attributable to the N-H proton and the hydroxy group of the naphthenic ring in the ^{1}H NMR spectrum, revealing that we are witnessing a deprotonation. The protons of the naphthenic ring appear at δ_H: 8.2-7.2 ppm. Using ^{1}H-^{1}H COSY and HSQC spectra, the final structure was elucidated and the naphthenic protons H-6 (δ_H: 7.43 ppm, m), H-1 (δ_H: 7.60 ppm, m) and H-2 (δ_H: 8.25 ppm, d, J=8.5 Hz) were correlated to the carbons C-6 (δ_C: 124.91 ppm), C-1 (δ_C: 129.03 ppm) and C-2 (δ_C: 121.34 ppm) (Figure 3).

Figure 3.

Using the HMBC spectrum, correlations between the proton H-11 and the carbons C-10 (δ_C: 109.29 ppm), C-5 (δ_C: 133.68 ppm) and C-9 (δ_C: 160.53 ppm) could be observed. In addition, the presence of C-9 in a weaker field indicates that the naphthenic ring is substituted in the ortho-position by a hydroxy group.

Finally, the complete elucidation was performed assigning the protons H-7 (δ_H: 7.95 ppm, d, J=9.0 Hz), H-8 (δ_H: 7.24 ppm, dd, J=14.9, 8.9 Hz) and H-3 (δ_H: 7.88 ppm, dd, J=8.2, 1.4 Hz) to the carbons C-7 (δ_C: 134.14 ppm), C-8 (δ_C: 119.99 ppm) and C-3 (δ_C: 129.82 ppm).

3.2. Cytotoxic activity of the extracts

Regarding the cytotoxicity of the *D. draco* extracts, the results showed that the aqueous (CC_{50}=91.20-96.60 μg/mL), dichloromethane (CC_{50}=87.30-85.40 μg/mL) and alkaloid-rich

dichloromethane (CC_{50}=84.70-85.80 μg/mL) extracts did not show relevant cytotoxicity (p=0.074) when compared to the positive control (Actinomycin D, CC_{50}=7.95 nM) in any of the cell lines (THP-1, NIH-3T3 and HaCaT) (Table 1).

Table 1.

3.3. Anti-inflammatory activities of the extracts

Concerning the anti-inflammatory capacity, the results showed that the dichloromethane (IC_{50}=60.80-58.90 μg/mL) and alkaloid-rich dichloromethane (IC_{50}=64.10-65.69 μg/mL) extracts presented a greater inhibitory activity of the production of NF-κB than the aqueous extract (IC_{50}=91.35-93.79 μg/mL) in all cell lines (Table 2).

Table 2.

On the other hand, the results concerning the activation of the Nrf2 factor confirmed that the dichloromethane (EC_{50}=22.53-24.75 μg/mL) and alkaloid-rich dichloromethane (EC_{50}=25.84-28.95 μg/mL) extracts presented statistically significant lower EC_{50} values (p<0.001) than the aqueous extract (EC_{50}=63.70-68.82 μg/mL) in all cell lines (Table 3).

Table 3.

3.4. Antimicrobial activities of the extracts

Regarding the antimicrobial capacity, the dichloromethane and alkaloid-rich dichloromethane extracts showed a statistically significant ZI (p<0.001) on the *E. coli*, *C.*

albicans and *S. aureus* type strains, with an IC_{50} of 27.19-29.37 μg/mL and 21.23-24.47 μg/mL, respectively (Table 4).

Table 4.

These results were confirmed by the MIC assay, where the extracts showed a MIC of 24.04-26.75 μg/mL (dichloromethane extract) and 18.58-19.92 μg/mL (alkaloid-rich dichloromethane extract), presenting a similar activity to the positive control (Ofloxacin, IC_{50}=10.00 μg/mL) (p=0.023) (Table 5).

Table 5.

3.5. Pro-proliferative activity of the extracts

Finally, in relation to the pro-proliferative properties (cell proliferation of NIH-3T3 fibroblasts and HaCaT keratinocytes), the dichloromethane (IC_{50}=36.43-37.16 μg/mL) and alkaloid-rich dichloromethane (IC_{50}=30.39-34.65 μg/mL) extracts showed a higher pro-proliferative activity when compared to the other extracts (Figure 4).

Figure 4.

Given that the dichloromethane and alkaloid-rich dichloromethane extracts had greater pharmacological potential, they were selected for further fractionation.

3.6. Cytotoxic activity of the fractions

The dichloromethane extract was fractionated using DCM/MeOH as the mobile phase, producing eleven fractions that were subjected to cytotoxicity, anti-inflammatory and antimicrobial assays. Table 1S shows the cytotoxicity results; first fractions showed low cytotoxicity while the last fractions were highly cytotoxic, and the **F2** fraction (CC_{50}=75.03-77.68 μg/mL) had the lowest cytotoxicity. **F2** had also statistically significant lower cytotoxicity than the other fractions.

The alkaloid-rich dichloromethane extract obtained through the liquid-liquid extraction technique was fractionated by column chromatography using the HEX, dioxane and MeOH solvents. Three fractions (1-3) were obtained. **F1´** and **F2´** had CC_{50} values between 71.56-76.32 μg/mL and 72.75-79.54 μg/mL, values which show a statistically significant lower cytotoxicity than the **F3´** (Table 6S).

3.7. Anti-inflammatory activities of the fractions

The anti-inflammatory results showed that the **F2** fraction (IC_{50}=44.40-44.70 μg/mL) has the highest inhibitory activity of the NF-κB production (Table 2S). Additionally, the results on the activation of the Nrf2 factor confirmed that the **F2** fraction (EC_{50}=13.20-14.90 μg/mL) has statistically significant lower EC_{50} values than the other fractions in all cell lines (Table 3S).

Concerning the anti-inflammatory capacity of the fractions obtained from the alkaloid-rich dichloromethane extract, the results showed that the **F1´** (IC_{50}=38.51-39.52 μg/mL) and **F2´** (IC_{50}=32.95-35.09 μg/mL) fractions had a higher inhibitory activity of the NF-κB production than the **F3´** fraction (IC_{50}=51.15-57.78 μg/mL) in all cell lines (Table 7S). Moreover, the results on the activation of the Nrf2 factor showed that the **F1´** (EC_{50}=6.13-6.27 μg/mL) and **F2´** (EC_{50}=4.31-5.63 μg/mL) fractions have statistically significant lower EC_{50} values than the **F3´** fraction (EC_{50}=15.68-19.82 μg/mL) in all cell lines (Table 8S).

515 *3.8. Antimicrobial activities of the fractions*

516 The **F2** fraction showed a statistically significant ZI, with an IC_{50} of 11.51-13.61 μg/mL
517 (Table 4S). This result was confirmed by the MIC assay, where the **F2** fraction showed a MIC
518 of 8.40-9.49 μg/mL, having an antimicrobial activity similar to the positive control (Ofloxacin,
519 IC_{50}=10.00 μg/mL) (p=0.095) (Table 5S).

520 Fractions **F1´** and **F2´** showed a statistically significant ZI, with an IC_{50} of 3.99-5.48
521 μg/mL and 2.36-3.17 μg/mL (Table 9S). These results were confirmed by the MIC assay, where
522 the fractions showed a MIC of 2.03-2.91 μg/mL (**F1´**) and 1.66-1.96 μg/mL (**F2´**). Both
523 fractions have a higher activity than the positive control (Ofloxacin, IC_{50}=10.00 μg/mL)
524 (p<0.001) (Table 10S).

525 Through the chromatographic separation of the **F2** fraction, a total of eight fractions
526 (F2.I-F2.VIII) were obtained, with **F2.VIII** (**Bexarotene**) as the most active fraction (Tables
527 11S-15S). Likewise, the chromatographic purification of the fractions **F1´-F2´** led to obtaining
528 **Taspine** and **2-hydroxy-1-naphthaldehyde isonicotinoyl hydrazone**, which were the most
529 active fractions.

530

531 *3.9. Cytotoxic activity of the compounds*

532 Table 6 shows the cytotoxicity of the pure compounds. **Bexarotene** (compound **1**,
533 CC_{50}=87.12-87.95 μM) had lower cytotoxicity than compounds **2-hydroxy-1-**
534 **naphthaldehyde isonicotinoyl hydrazone** (compound **3**, CC_{50}=71.58-75.41 μM) and **Taspine**
535 (compound **2**, CC_{50}=66.77-69.31 μM).

536

537 **Table 6.**

538

539

3.10. Anti-inflammatory activities of the compounds

The three compounds showed an inhibitory capacity of the NF-κB production higher than the positive control (Celastrol, IC_{50}=7.43 μM), with IC_{50} values of 0.10-0.13 μM (compound **1**), 0.22-0.24 μM (compound **2**) and 3.75-4.78 μM (compound **3**) (Figure 5).

Figure 5.

Moreover, regarding the stimulation of Nrf2, effective concentrations of 5.34-5.43 *n*M (compound **1**), 163.20-169.20 *n*M (compound **2**) and 300.82-315.56 *n*M (compound **3**) were obtained. There are no previous reports on the effect of these three compounds on the production of Nrf2. However, although the isolated compounds showed Nrf2 stimulating activity, they are not better than the positive control (CDDO-Me, IC_{50}=0.11 *n*M). Compound **1** is the one that has the highest Nrf2 stimulation potential, and as such is the one that would be the closest to the values displayed by the positive control (Figure 6).

Figure 6.

3.11. Pro-proliferative activity of the compounds

It was observed that compound **1** (IC_{50}=8.62-8.71 *n*M) had a higher pro-proliferative activity, similar to the positive control (FSB, 100%). Compounds **2** (IC_{50}=166-171 *n*M) and **3** (IC_{50}=469-486 *n*M) showed a pro-proliferative activity of 75% and 65% (Figure 7).

Figure 7.

565 *3.12. Antimicrobial activities of the compounds*

566 The three compounds showed a statistically significant ZI in the *E. coli*, *C. albicans* and
567 *S. aureus* strains, with an IC_{50} of 0.14-0.19, 0.41-0.49 and 4.69-4.86 μM, respectively (Figure
568 8). The ZI of compound **1** was higher than that of Ofloxacin (positive control).

569

570 **Figure 8.**

571

572 These results were corroborated through the minimum inhibitory concentration (MIC)
573 assay, obtaining MIC values of 0.12-0.16 μM (compound **1**), 0.31-0.39 μM (compound **2**) and
574 3.96-3.99 μM (compound **3**). Thus, the compounds showed higher antimicrobial activity than
575 the positive control (Ofloxacin, IC_{50}=27.67 μM) (Figure 9).

576

577 **Figure 9.**

578

579 **4. Discussion**

580 The three isolated compounds have been described in previous works. However, this is
581 the first time they have been isolated in the *D. draco* species. In this sense, compound **1** was
582 first synthesised in 1993 by Ligand Pharmaceuticals Inc. (Boehm *et al*., 1993). In relation to
583 compound **2**, it has been isolated from different plant species such as: *Leontice eversmannii*
584 (Platonova *et al*., 1953), *Croton Lechleiri* (Perdue *et al*., 1979) and *Magnolia liliflora*
585 (Talapatra *et al*., 1982). Finally, in relation to compound **3**, it was synthesised for the first time
586 by Sacconi (1953).

587 There are no studies regarding the cytotoxicity of *D. draco* extracts. However, there is a
588 toxicity study that reported that the ethyl acetate extract from *D. draco* did not show toxicity
589 at a dose of 8000 mg/kg body weight (lethal dose 50) in Sprague Dawley rats. Macroscopic

observation of the liver and kidneys showed that there were no abnormalities and that the organ weights were within normal values (Yunita & Mursyid, 2019). Relating the toxicity data obtained from previous work and the cytotoxicity results obtained in our work, we can conclude that there is a relationship between cytotoxicity/toxicity and the polarity of the extracts. In this sense, the apolar extracts showed greater cytotoxicity/toxicity than the polar extracts.

Regarding the compounds isolated from the dichloromethane and alkaloid-rich dichloromethane extracts, previous studies have shown that compound **1** was not cytotoxic in the PC12 cell lines (CC_{50}>100 μM) (Wang *et al*., 2019); in our study we confirmed that this compound was not cytotoxic in any of the cell lines. Compound **2** did not show relevant cytotoxicity confirming the results previously reported in KB tumour (CC_{50}=0.39 μg/mL) and V-79 (CC_{50}=0.17 μg/mL) cell lines by Itokawa *et al.* (1991). Finally, compound **3** has been reported as cytotoxic against different tumour cell lines confirming the results of Green *et al*. (2001) (IC_{50}=0.65-2.3 μM). Our study shows that the compound **3** is not cytotoxic. This contradiction between our results and those reported in previous reports may be because the tests were conducted in different cell lines, with different morphological features.

On the other hand, in relation to the anti-inflammatory activity of the extracts of *D. draco*, previous studies have shown that the ethanolic extract of *D. draco* presented anti-inflammatory activity (inhibition of the production of interleukin 1β, TNF-α and NF-κB) in a range of concentrations between 10-200 μg/mL (Choy *et al.,* 2008). Furthermore, the ethanolic extract of *D. draco* stimulated the production of HO-1 (Heme Oxygenase 1) which is directly related to the suppression of NF-κB and to the activation of Nrf2 (Wardyn *et al.,* 2015). This potential was confirmed in our case through the methanolic extract that presented an inhibitory activity of NF-κB (IC_{50}=46.26-49.39 μg/mL) and a stimulating activity of Nrf2 (IC_{50}=10.47-17.69

614 μg/mL). However, this extract was not studied due to its cytotoxicity (CC_{50}=52.20-54.00
615 μg/mL).

616 Regarding the anti-inflammatory activity of the compounds, previous studies have
617 reported the inhibition potential over the NF-κB production of compound **1**, inhibiting the
618 phosphorylation of Iκβα in chondriosomes (Zha *et al*., 2020). Concerning compounds **2** and **3**,
619 there are no reports on their effect on the production of NF-κB. However, there are reports that
620 mention that compound **2** has anti-inflammatory activity (Perdue *et al*., 1979; Raintree
621 Nutrition, 2007) and compound **3** attenuates ROS production (Wang *et al*., 2016).

622 The mechanism of action of compounds **2** and **3** on the NF-κB pathway is unknown.
623 However, our results show that these compounds are better than the positive control (Celastrol).
624 If we account for the fact that the mechanism of action of Celastrol is through the suppression
625 of the degradation of Iκβα and inhibition of the translocation of p65 of the nucleus (Youn *et*
626 *al*., 2014), we can deduct that compounds **2** and **3** act on these factors on the NF-κB inhibition
627 pathway.

628 On the other hand, analysing the mechanism of action of the positive control (CDDO-
629 Me) on the Nrf2 pathway, we observe that it acts by generating bonds with the thiol groups of
630 the Keap-1 unit, which leads to the release of the Nrf2 unit. This release leads to subsequent
631 nuclear transcription and the production of a coordinated antioxidant and anti-inflammatory
632 response (Wang *et al*., 2014). Based on this premise, a similar mechanism of action on the Nrf2
633 pathway can be assumed for the three compounds.

634 Additionally, the anti-inflammatory activity of the compounds can be related to their
635 lipophilic capacity. This concerns the partition coefficient of the three compounds. The higher
636 the partition coefficient (Log P), the more hydrophobic the compound is and, therefore, it is
637 better distributed in hydrophobic environments such as the lipid bilayers that make up cells

(Kapustikova *et al*., 2018). Based on this premise, compound **1** is the most absorbable since it has a Log P of 6.86 (compound **2**, Log P of 3.18, and compound **3**, Log P of 2.18).

We can conclude that both the inhibition of the NF-κB nuclear factor and the activation of the Nrf2 factor are crucial for the anti-inflammatory action during the pro-proliferative process (Ahmed *et al*., 2017). The isolated compounds have shown both activities.

In relation to the antimicrobial activity of extracts of *D. draco*, Wahyuni *et al.* (2018) reported that hexane (ZI=10.57 μg/mL), ethyl acetate (ZI=15.05 μg/mL, MIC=1.0 mg/mL) and methanol (ZI=13.40 μg/mL, MIC=0.5 mg/mL) extracts of *D. draco* have antimicrobial activity against *S. aureus*. Our study shows that the hexane and methanolic extracts have ZI of 96.56 μg/mL and 54.67 μg/mL against the *S. aureus* strain, with MIC results of 87.33 and 48.78 μg/mL, respectively. Furthermore, these extracts showed similar activities against *E. coli* and *C. albicans* strains. Thus, our results confirm the activity of *D. draco* extracts on Gram-positive bacteria (*S. aureus*). Moreover, our study highlights the antimicrobial activity on Gram-negative bacteria (*E. coli*) and yeasts (*C. albicans*).

Regarding the antimicrobial activity of the compounds, there are previous studies on the antimicrobial activity of compound **1** against Gram-positive bacteria (*P. acnes*) (Aranegui & García-Cruz, 2012). There are no previous reports of the antimicrobial activity of compound **2**. Concerning compound **3**, its antimicrobial activity was reported against *S. aureus* (Gram-positive), *E. coli* (Gram-negative) and *C albicans* (yeast), with an inhibitory concentration of 2.07, 2.07 and 2.37 μM, respectively (Judge *et al*., 2011). These results are similar to those obtained in the current report.

Analysing the mechanism of antimicrobial action of Ofloxacin, we observed that it inhibits topoisomerases II, IV and DNA gyrase that are necessary to complete the cycle of bacterial division (Todd & Faulds, 1991). In this sense, our compounds can have a similar mechanism of action, however this should be further analysed in future studies.

663 Finally, we observed that the pro-proliferative activity of compound **1** is due to its
664 retinoid type structure; compound **1** produces an increase of fibroplasia and angiogenesis
665 (Fernández & Armario, 2003). In relation to compound **2**, there are reports on its pro-
666 proliferative activity in the early stages of the wound. This is because it promotes the migration
667 of fibroblasts at 50 *p*g/mL (Porras-Reyes *et al*., 1993). However, compound **2** has been shown
668 to have a higher pro-proliferative activity in its salt form (De Fátima *et al.,* 2008). Furthermore,
669 *in vitro* assays have shown that, after its application, compound **2** produces an acceleration in
670 the growth of collagen, capillaries (angiogenesis), as well as an increase in the autocrine of
671 TGF-β, and the EGF (Epidermal Growth Factor) in fibroblasts (Raintree Nutrition, 2007).
672 Concerning compound **3**, Walcourt *et al*. (2013) showed that it is an iron chelator. Iron
673 chelators are used as pharmacological agents because they suppress the lack of iron,
674 accelerating the pro-proliferative process (Wright *et al*., 2014).
675 *In vitro* studies (cell cultures) provided us with information on the possible mechanism
676 of anti-inflammatory and pro-proliferative activities of the extracts, fractions and compounds
677 isolated from *Daemonorops draco* (Willd.) Blume species. However, to support the idea of
678 action on NF-κB (suppression of phosphorylation of IKKαβ) and pro-proliferative activity, it
679 would be beneficial to perform *in vivo* and mechanistic studies.
680
681 **5. Conclusion**
682 This report has confirmed the anti-inflammatory, pro-proliferative and antimicrobial
683 activities of the *D. draco* resin. Moreover, this study is the first report isolating Bexarotene (**1**),
684 Taspine (**2**) and 2-hydroxy-1-naphthaldehyde isonicotinoyl hydrazone (**3**) from the
685 *Daemonorops draco* (Willd.) Blume species. For compounds **1** and **3**, it is the first time that
686 they have been isolated from a natural product, given that previous authors have only obtained
687 these compounds through chemical synthesis. Although compound **2** has been considered a

biomarker of the *Croton lechleri* species, this work confirms its presence in the *D. draco* species. The chemical relation between these species and other "Dragon´s blood" species should be analysed in future studies.

The current report has shown that the three compounds could be used to develop topical treatments seen as healing alternatives to those already on the market. In addition, future reports on these compounds could use them for unveiling the relation between structure and activity (SAR). In addition to these three compounds, bio-guided isolation should look for new compounds since the *D. draco* species has not been comprehensively studied, and our study is only a first step towards such efforts.

Declaration of interest

The authors declare no conflict of interest.

Author contributions

S.S.C.J and A.T.L performed the phytochemical analysis and isolation of compounds. O.D.M performed biological experiments and helped with the manuscript writing and figures preparation. I.M.P. helped with the statistical analysis of the data. R.S.A conceived and supervised the study, provided the plant materials and helped with the manuscript writing. A.T.L. conceived and supervised the study, performed the experiments and the statistical analysis and wrote and edited the manuscript and the figures. All authors read and approved the final manuscript.

Acknowledgments

This work was supported by the National Herbarium of Bolivia, the Fundación de la Universidad Autónoma de Madrid (FUAM).

Appendix A. Supplementary data

^{1}H-NMR, ^{13}C-NMR, ^{1}H-^{1}H COSY, HMQC, HSQC, HMBC and MS spectra for extracts and isolated compounds.

References

Agyare, C., Akindele, A.J., Steenkamp, V. 2019. Natural Products and/or Isolated Compounds on Wound Healing. Evid Based Complement Alternat Med 2019, 4594965. https://doi.org/10.1155/2019/4594965.

Ahmed, S.M., Luo, L., Namani A, Wang. X.J., Tang. X. 2017. Nrf2 signaling pathway: Pivotal roles in inflammation. Biochim Biophys Acta Mol Basis Dis 1863(2), 585-597. https://doi.org/10.1016/j.bbadis.2016.11.005.

Altieri, A., Franceschin, M., Nocioni, D., Alvino, A., Casagrande, V., Scarpati, L., Bianco, A. 2013. Total Synthesis of Taspine and a Symmetrical Analogue : Study of Binding to G-Quadruplex DNA by ESI-MS. Eur J Org Chem 191-196. https://doi.org/10.1002/ejoc.201201034.

Ambrozova, N., Ulrichova, J., Galandakova, A. 2017. Models for the study of skin wound healing. The role of Nrf2 and NF-κB. Biomed Pap Med Fac Univ Palacky Olomouc Czech Repub 161, 1-13. https://doi.org/10.5507/bp.2016.063.

Apaza, T.L., Rumbero, S.Á., Orosco, G.Ó., Ortega, D.M. 2020. Antimicrobial compounds isolated from *Tropaeolum tuberosum*. Nat Prod Res 1-5. https://doi.org/10.1080/14786419.2019.1710700.

Aranegui, B., García-Cruz, A. 2012. Topical Retinoids, in: Conde-Taboada, A. (Ed.), Dermatological Treatments. Madrid, pp. 125-152.

737 Ashrafi, M., Baguneid, M., Bayat, A. 2016. The role of neuro mediators and innervation in
738 cutaneous wound healing. Acta Derm Venereol 96, 587-97.
739 https://doi.org/10.2340/00015555-2321.
740 Boehm, M.F., Heyman, R.A., Zhi, L. (1993, October 22). USA Patent No. WO9321146.
741 Cavaillon, J.M. 2018. Exotoxins and endotoxins: Inducers of inflammatory cytokines. Toxicon
742 149, 45-53. https://doi.org/10.1016/j.toxicon.2017.10.016.
743 Cheng, B., Zhang, S., Zhu, L., Zhang, J., Li, Q., Shan, A., He, L. 2009. Facile and efficient
744 total synthesis of taspine. Synthesis (Stuttg) 2501-2504. https://doi.org/10.1055/s-0029-
745 1217393.
746 Choy, C.S., Hu, C.M., Chiu, W.T., Lam, C.S.K., Ting, Y., Shin-Han Tsai, S.H., Wang, T.C.
747 2008. Suppression of lipopolysaccharide-induced of inducible nitric oxide synthase and
748 cyclooxygenase-2 by Sanguis Draconis, a dragon's blood resin, in RAW 264.7 cells. J
749 Ethnopharmacol 115, 455-462. https://doi.org/10.1016/j.jep.2007.10.012.
750 De Fátima, A., Modolo, L.V., Andréia, Sanches, A.C., Porto, R.R. 2008. Wound Healing
751 Agents: The Role of Natural and Non-Natural Products in Drug Development. Mini-Rev
752 Med Chem 8, 879-888. 10.2174/138955708785132738
753 Eichenfield, D.Z., Troutman, T.D., Link, V.M., Lam, M., Cho, H., Gosselin, D., Spann, N.J.,
754 Lesch, H.P., Tao, J., Muto, J., Gallo, R.L., Evans, R.M., Glass, C.K. 2016. Tissue damage
755 drives co-localization of NF-κB, Smad3, and Nrf2 to direct Rev-erb sensitive wound
756 repair in mouse macrophages. Elife 5, e13024. https://doi.org/10.7554/eLife.13024.
757 Fazil, M., Nikhat, S. 2020. Topical medicines for wound healing: A systematic review of Unani
758 literature with recent advances. J Ethnopharmacol 257, 112878.
759 https://doi.org/10.1016/j.jep.2020.112878.
760 Fernández, J.M., Armario, J.C. 2003. Retinoides en dermatología. Med Cutan Iber Lat Am
761 31(5), 271-294.

762 Georgescu, M., Marinas, O., Popa, M., Stan, T., Lazar, V., Bertesteanu, S.V., and Chifiriuc,
763 M.C. 2016. Natural Compounds for Wound Healing. In: Fonseca C. Worldwide Wound
764 Healing. https://doi.org/10.5772/65652.
765 Gonzalez, A.C., Costa, T.F., Andrade, Z.A., Medrado, A.R. 2016. Wound healing-A literature
766 review. An Bras Dermatol 91, 614-620. https://doi.org/10.1590/abd1806-
767 4841.20164741.
768 Gottrup, F., Apelqvist, J., Bjarnsholt, T., Cooper, R., Moore, Z., Peters, E.J., Probst, S. 2013.
769 EWMA document: antimicrobials and non-healing wounds. Evidence, controversies and
770 suggestions. J Wound Care 22, S1-S89. https://doi.org/10.12968/jowc.2013.22.Sup5.S1.
771 Green, D.A., Antholine, W.E., Wong, S.J., Richardson, D.R., Chitambar, C.R. 2001. Inhibition
772 of Malignant Cell Growth by 311, a Novel Iron Chelator of the Pyridoxal Isonicotinoyl
773 Hydrazone Class: Effect on the R2 subunit of Ribonucleotide Reductase. Clin Cancer
774 Res 7 (11), 3574-3579.
775 Gupta, D., Bleakley, B., Gupta, R.K., 2007. Dragon's blood: Botany, chemistry and therapeutic
776 uses. J Ethnopharmacol 115, 361-380. https://doi.org/10.1016/j.jep.2007.10.018.
777 Hiebert, P., Werner, S. 2019. Regulation of wound healing by the nrf2 transcription factor-
778 more than cytoprotection. Int J Mol Sci 20. https://doi.org/10.3390/ijms20163856.
779 Hop, H.T., Reyes, A.W.B., Huy, T.X.N., Arayan, L.T., Min, W.G., Lee, H.J., Rhee, M.H.,
780 Chang, H.H., Kim, S. 2017. Activation of NF-kB-Mediated TNF-Induced Antimicrobial
781 Immunity Is Required for the Efficient Brucella abortus Clearance in RAW 264.7 Cells.
782 Front Cell Infect Microbiol 7, 437. https://doi.org/10.3389/fcimb.2017.00437.
783 Hülpüsch, C., Tremmel, K., Hammel, G., Bhattacharyya, M., de Tomassi, A., Nussbaumer, T.,
784 Neumann, A. U., Reiger, M., Traidl-Hoffmann, C. 2020. Skin pH-dependent
785 *Staphylococcus aureus* abundance as predictor for increasing atopic dermatitis severity.

786 Allergy 10.1111/all.14461. Advance online publication.
787 https://doi.org/10.1111/all.14461.
788 Itokawa, H., Ichihara, Y., Mochizuki, M., Enomori, T., Morita, H., Shirota, O., Inamatsu, M.,
789 Takeya, K. 1991. A Cytotoxic Substance from Sangre de Grado. Chem Pharm Bull 39(4),
790 1041-1042. https://doi.org/10.1248/cpb.39.1041
791 Judge, V., Narasimhan, B., Ahuja, M., Sriram, D., Yogeeswari, P., De Clercq, E.,
792 Pannecouque, C., Balzarini, J. 2011. Isonicotinic acid hydrazide derivatives: synthesis,
793 antimicrobial activity, and QSAR studies. Med Chem Res 21, 1451-1470.
794 https://doi.org/10.2174/157340613804488404.
795 Kabashima, K., Honda, T., Ginhour, F., Egawa, G. 2019. The immunological anatomy of the
796 skin. Nat Rev Immunol 19, 19-30. https://doi.org/10.1038/s41577-018-0084-5.
797 Kapustikova, I., Bak, A., Gonec, T., Kos, J., Kozik, V., Jampilek, J. 2018. Investigation of
798 Hydro-Lipophilic Properties of N-Alkoxyphenylhydroxynaphthalenecarboxamides.
799 Molecules, 23, 1635. https://doi.org/10.3390/molecules23071635.
800 Kashem S.W., Kaplan, D.H. 2016. Skin Immunity to *Candida albicans*. Trends Immunol
801 37(7), 440-450. https://doi.org/10.1016/j.it.2016.04.007.
802 Kuo, P.C., Hung, H.Y., Hwang, T.L., Du, W.K., Ku, H.C., Lee, E.J., Tai, S.H., Chen, F.A.,
803 Wu, T.S. 2017. Anti-inflammatory Flavan-3-ol-dihydroretrochalcones from
804 *Daemonorops draco*. J Nat Prod 80, 783-789.
805 https://doi.org/10.1021/acs.jnatprod.7b00039.
806 Lawrence, T. 2009. The nuclear factor NF-kappaB pathway in inflammation. Cold Spring Harb
807 Perspect Biol 1, a001651. https://doi.org/10.1101/cshperspect.a001651.
808 Merlini, L., Nasini, G. 1976. Constituents of dragon's blood. II. Structure and oxidative
809 conversion of a novel secobiflavonoid. J Chem Soc Perkin Trans I 1, 1570.
810 https://doi.org/10.1039/P19760001570.

811 Nasini, G., Piozzi F. 1981. Pterocarpol and triterpenes from *Daemonorops draco.*
812 Phytochemistry 20, 514-516. https://doi.org/10.1016/S0031-9422(00)84180-1.
813 Opal, S.M., DePalo, V.A. 2000. Anti-inflammatory cytokines. Chest 117, 1162-1172.
814 https://doi.org/10.1378/chest.117.4.1162.
815 Perdue, G.P., Blomster, R.N., Blake, D.A., Farnsworth, N.R. 1979. South American Plants 11:
816 Taspine Isolation and Anti-Inflammatory Activity. J Pharm Sci 68(1), 124-126.
817 https://doi.org/10.1002/jps.2600680145.
818 Petkovsek, Z., Elersic, K., Gubina, M., Zgur-Bertok, D., Starcic Erjavec, M. 2009. Virulence
819 potential of *Escherichia coli* isolates from skin and soft tissue infections. J Clin Microbiol
820 47(6), 1811-1817. https://doi.org/10.1128/JCM.01421-08.
821 Piozzi, F., Passannanti, S., Paternostro, M. P., Nasini, G. 1974. Diterpenoid resin acids of
822 *Daemonorops draco*. Phytochemistry 13, 2231-2233. https://doi.org/10.1016/0031-
823 9422(74)85033-8.
824 Platonova, T.F., Kuzovkov, A.D., Massagetov, P.S. 1953. Alkaloids of plants, Leontice
825 eversmannii. I. New alkaloid taspine and alkaloid isoleontine. Preparation of leontidane
826 and isoleontane. Russ J Gen Chem 23, 880-886.
827 Porras-Reyes, B.H., Lewis, W.H., Roman, J., Simchowitz, L., Mustoe, T.A. 1993.
828 Enhancement of Wound Healing by the Alkaloid Taspine Defining Mechanism of
829 Action. Ex Biol Med 203(1), 18-25. https://doi.org/10.3181/00379727-203-43567.
830 Proksch, E. 2018. PH in nature, humans and skin. J Dermatology 45, 1044-1052.
831 https://doi.org/10.1111/1346-8138.14489.
832 Purwanti, S., Wahyuni, W.T., Batubara, I. 2019. Antioxidant Activity of *Daemonorops draco*
833 Resin. J. Kim. Sains dan Apl. 22, 179. https://doi.org/10.14710/jksa.22.5.179-183.

834 Raintree Nutrition, I., 2007. Biological Activities for Sangre de Grado (*Croton lechleri*)
835 [WWW Document]. URL https://rain-tree.com/sangre-de-grado-activity.pdf (accessed
836 9.12.20).
837 Sacconi, L. 1953. Chemical reactions leading to the formation of complexes. Polymeric
838 polynuclear nickel complexes with hydrazides of β-pyridine- and γ-pyridinecarboxylic
839 acids. Gazz Chim Ital 83, 894-904.
840 Sami, D.G., Heiba, H.H., Abdellatif, A. 2019. Wound healing models: A systematic review of
841 animal and non-animal models. Wound Med 24, 8-17.
842 https://doi.org/10.1016/j.wndm.2018.12.001.
843 Sulasmi, I.S. 2012a. Jernang Rattan (*Daemonorops Draco*) Management by Anak Dalam Tribe
844 in Jebak Village, Batanghari, Jambi Province. J Biol Divers, 13, 151-160.
845 https://doi.org/10.13057/biodiv/d130309.
846 Sulasmi, I.S., 2012b. The population of Jernang rattan (*Daemonorops draco*) in Jebak Village,
847 Batanghari District, Jambi Province, Indonesia. J Biol Divers 13, 205-213.
848 https://doi.org/10.13057/biodiv/d130407.
849 Talapatra, B., Chaudhuri, P.K., Talapatra, S.K. 1982. (-)-Maglifloenone, a novel
850 spirocyclohexadienone neolignan and other constituents form *Magnolia lilliflora*.
851 Phytochemistry 21, 747-750. https://doi.org/10.1016/0031-9422(82)83180-4.
852 Todd, P.A., Faulds, D.1991. Ofloxacin: A Reappraisal of its Antimicrobial Activity,
853 Pharmacology and Therapeutic Use. Drugs 42(5), 825-876.
854 Tsacheva, I., Rostan, J., Iossifova, T., Vogler, B., Odjakova, M., Navas, H., Kostova, I.,
855 Kojouharova, M., Kraus, W. 2004. Complement Inhibiting Properties of Dragon' s Blood
856 from Croton draco. Z Naturforsch C J Biosci 59, 528-532. https://doi.org/10.1515/znc-
857 2004-7-814.

858 Vermeulen, H., Westerbos, S.J., Ubbink, D.T. 2010. Benefit and harm of iodine in wound care:
859 a systematic review. J Hosp Infect 76, 191-199.
860 https://doi.org/10.1016/j.jhin.2010.04.026.
861 Wahyuni, W.T., Purwanti, S., Batubara, I. 2018. Antibacterial and Antibiofilm Activity of
862 *Daemonorops draco* Resin. Biosaintifika J Biol Biol Educ 10, 138-144.
863 https://doi.org/10.15294/biosaintifika.v10i1.13554.
864 Walcourt, A., Kurantsin-Mills, J., Kwagyan, J., Adenuga, B.B., Kalinowski, D.S., Lovejoy,
865 D.B., Lane, J.R., Richardson, D.R. 2013. Anti-plasmodial activity of aroyl hydrazone
866 and thiosemicarbazone iron chelators: Effect on erythrocyte membrane integrity, parasite
867 development and the intracellular labile iron pool. J Inorg Biochem 129, 43-51.
868 https://doi.org/10.1016/j.jinorgbio.2013.08.007.
869 Wang, G., Tang, C., Yan, G., Feng, B. 2016. Gene Expression Profiling of H9c2 Cells
870 Subjected to H2O2-Induced Apoptosis with/without AF-HF001. Biol Pharm Bull 39(2),
871 207-214. https://doi.org/10.1248/bpb.b15-00601.
872 Wang, W., Nakashima, K.I., Hirai, T. Inoue, M. 2019. Neuroprotective effect of naturally
873 occurring RXR agonists isolated from *Sophora tonkinensis* Gagnep. on
874 amyloid‐β‐induced cytotoxicity in PC12 cells. J Nat Med 73, 154–162.
875 https://doi.org/10.1007/s11418-019-01305-8.
876 Wang, Y.Y., Yang, Y.X., Zhe, H., He, Z.X., Zhou, S.F. 2014. Bardoxolone methyl (CDDO-
877 Me) as a therapeutic agent: an update on its pharmacokinetic and pharmacodynamic
878 properties. Drug Des Dev Ther 8, 2075-2088. https://doi.org/10.2147/DDDT.S68872.
879 Wardyn, J.D., Ponsford, A.H., Sanderson, C.M. 2015. Dissecting molecular cross-talk between
880 Nrf2 and NF-κB response pathways. Biochem Soc Trans 43, 621-626.
881 https://doi.org/10.1042/BST20150014.

882 Wright, J.A., Richards, T., Srai, S.K. 2014. The role of iron in the skin and cutaneous wound
883 healing. Front Pharmacol 5, 156. https://doi.org/10.3389/fphar.2014.00156.
884 Youn, G.S., Kwon, D.J., Ju, S.M., Rhim, H., Yong Soo Bae, Y.S., Choi, S.Y., Park, J. 2014.
885 Celastrol ameliorates HIV-1 Tat-induced inflammatory responses via NF-kappaB and
886 AP-1 inhibition and heme oxygenase-1 induction in astrocytes. Toxicol Appl Pharm 280,
887 42-52. https://doi.org/10.1016/j.taap.2014.07.010.
888 Yunita, F., Mursyid, L. 2019. Acute Toxicity Test of Jernang Resin Extract (*Daemonorops*
889 *Draco* Willd.) on Male White Rats Sprague Dawley Strain. Indones J Sci Technol 2(2),
890 2615-367.
891 Zha, Z., Han, Q., Huo, S. 2020. The protective effects of bexarotene against advanced glycation
892 end-product (AGE)-induced degradation of articular extracellular matrix (ECM). Artif
893 Cells Nanomed Biotechnol 48(1), 1-7. https://doi.org/10.1080/21691401.2019.1699802.
894 Zhao, R., Liang, H., Clarke, E., Jackson, C., Xue, M. 2016. Inflammation in Chronic Wounds.
895 Int J Mol Sci 17, 2085. https://doi.org/10.3390/ijms17122085.
896 Ziltener, P., Reinheckel, T., Oxenius, A. 2016. Neutrophil and alveolar macrophage-mediated
897 innate immune control of *Legionella pneumophila* lung infection via TNF and ROS.
898 PLoS Pathog 12, e1005591. https://doi.org/10.1371/journal.ppat.1005591.

Figure captions

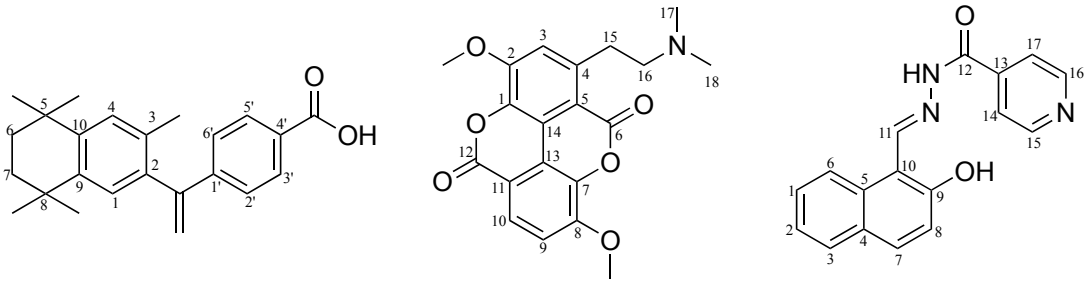

(1) **(2)** **(3)**

Figure 1. The chemical structures of triterpenoids from *D. draco*. (**1**) Bexarotene; (**2**) Taspine; (**3**) 2-hydroxy-1-naphthaldehyde isonicotinoyl hydrazone.

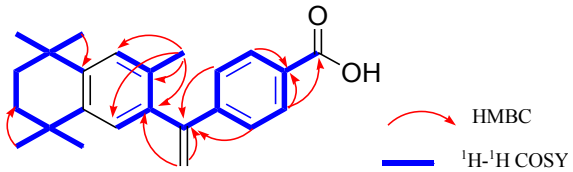

Figure 2. Structural correlation of compound **1**.

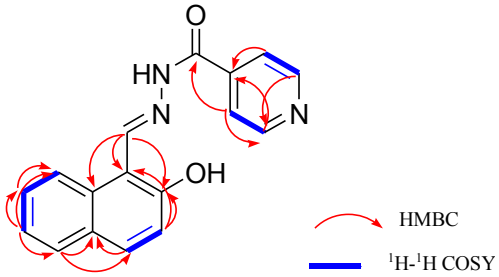

Figure 3. Structural correlation of compound **3**.

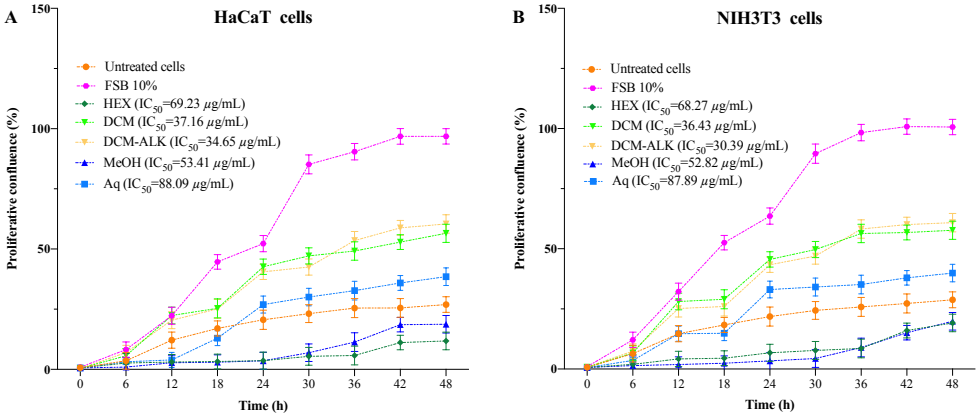

Figure 4. Effect of extracts from *D. draco* on pro-proliferative activity in HaCaT (**A**) and NIH3T3 (**B**) cells.

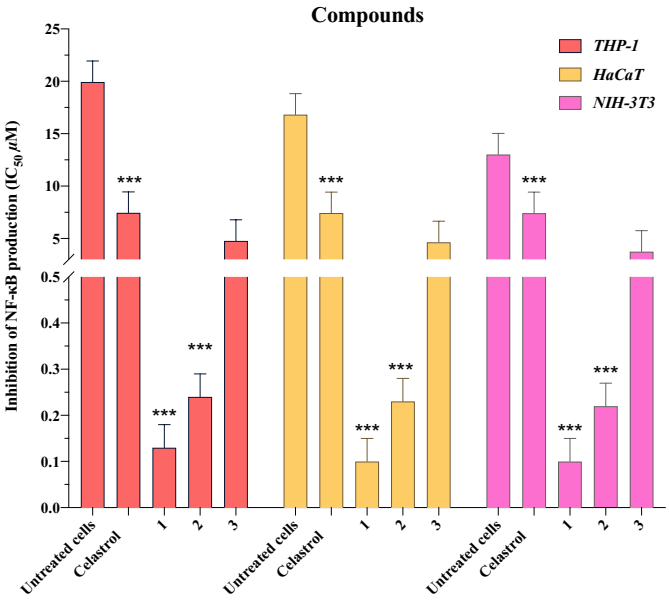

Figure 5. IC_{50s} of the inhibition of NF-κB production, calculated for the compounds from *D. draco* at 48 h. IC_{50} was calculated using Prism v8.4.0 (GraphPad Software) using non-linear regression, dose-response curves. CI95%: Confidence interval 95%/Tukey's multiple comparisons test (p<0.001).

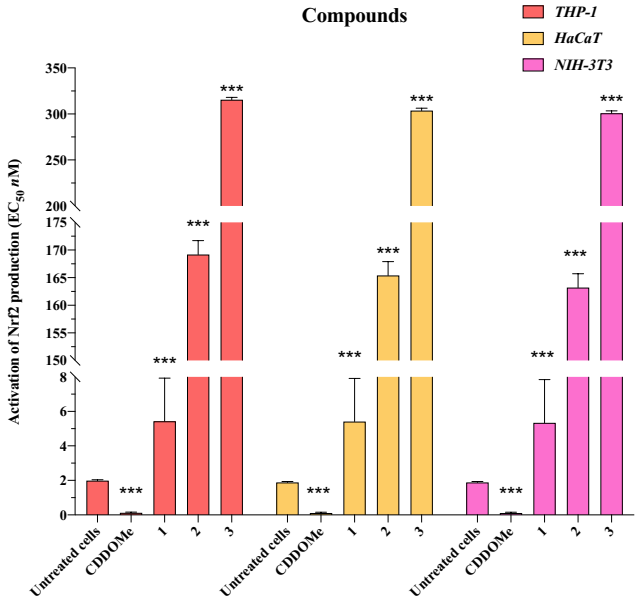

Figure 6. EC_{50s} of the activation of Nrf2 production, calculated for the compounds from *D*. draco at 48 h. EC_{50} was calculated using Prism v8.4.0 (GraphPad Software) using non-linear regression, dose-response curves. CI95%: Confidence interval 95%/Tukey's multiple comparisons test (p<0.001).

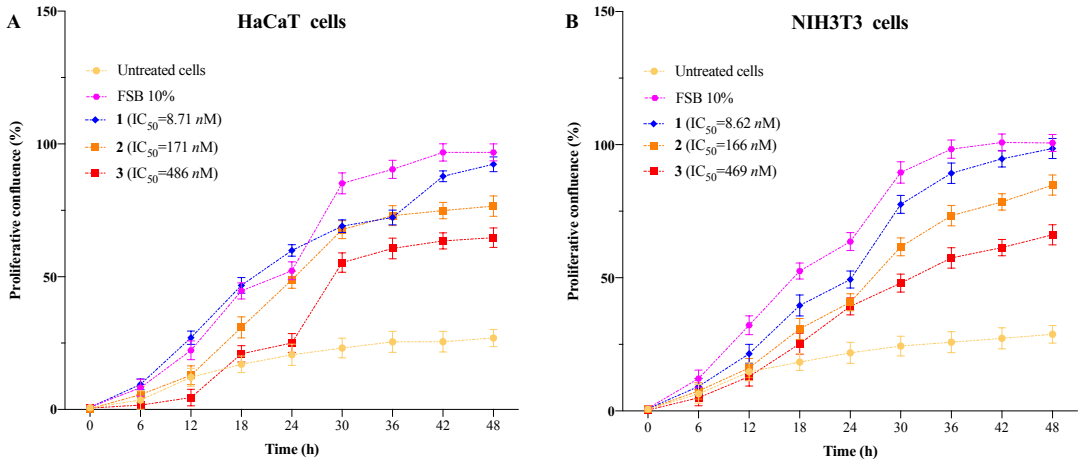

Figure 7. Effect of compounds from *D. draco* on pro-proliferative activity in HaCaT (**A**) and NIH3T3 (**B**) cells.

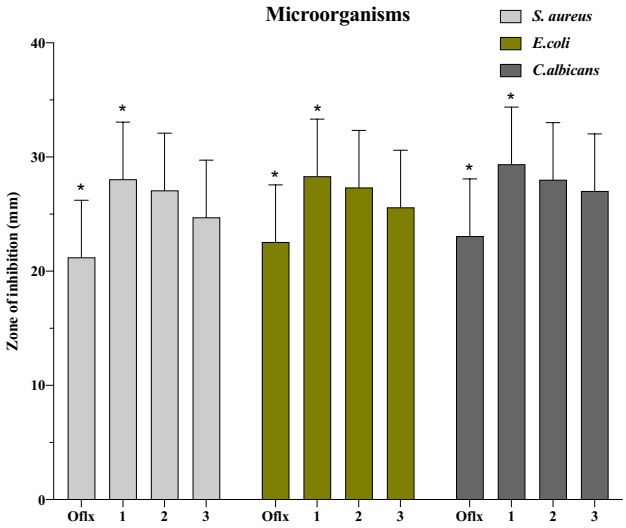

Figure 8. *In vitro* culture plates (agar cup plate method) of *D. draco* compounds showing the zone of inhibition (ZI) concentration against different strains of microorganisms at 48 h. IC_{50s} of the ZI was calculated using Prism v8.4.0 (GraphPad Software) using non-linear regression, dose-response curves. CI95%: Confidence interval 95%/Tukey's multiple comparisons test (p<0.001).

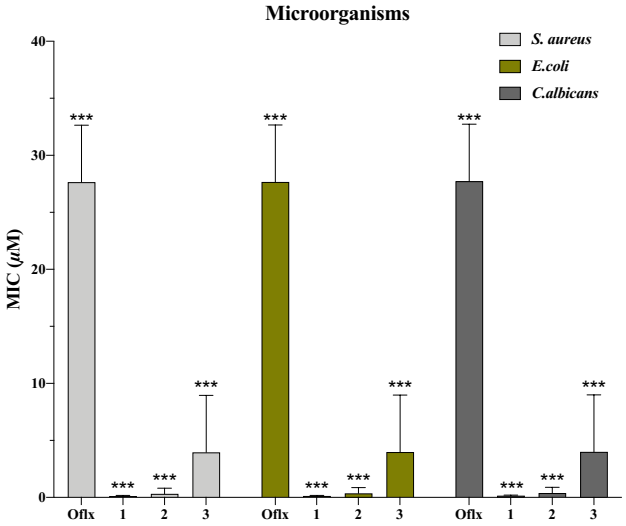

Figure 9. Minimum inhibitory concentration (MIC) of *D. draco* compounds against different strains of microorganisms at 48 h. MIC was calculated using Prism v8.4.0 (GraphPad Software) using non-linear regression, dose-response curves. CI95%: Confidence interval 95%/Tukey's multiple comparisons test ($p<0.001$).

Table captions

Table 1. CC_{50s} of the LDH (Cytotoxicity) assays calculated for the extracts from *D. draco* CC_{50} was calculated using Prism v8.4.0 (GraphPad Software) using non-linear regression, dose-response curves. CI95%: Confidence interval 95%/Tukey's multiple comparisons test (p<0.001***).

Extracts	Cytotoxicity (CC_{50} μg/mL) at 48 h (CI95%, R2)		
	THP-1	HaCaT	NIH-3T3
Untreated cells	98.26 (93.43 to 103.65, 0.9868)	99.37 (94.13 to 104.40, 0.9868)	98.49 (93.40 to 103.45, 0.9868)
DMSO	20.29 (15.94 to 25.91, 0.9615)	20.09 (15.56 to 24.59, 0.9615)	20.05 (15.41 to 25.11, 0.9615)
Actinomycin D*	7.97 (2.24 to 11.35, 0.9697)	7.95 (2.27 to 12.42, 0.9697)	7.92 (2.54 to 12.74, 0.9697)
HEX	75.00 (70.94 to 80.54, 0.9842)	73.30 (68.93 to 78.91, 0.9842)	73.05 (68.45 to 78.75, 0.9842)
DCM	**87.30 (82.65 to 92.26, 0.9827)**	**86.50 (81.59 to 91.63, 0.9827)**	**85.40 (80.45 to 90.49, 0.9827)**
MeOH	54.00 (49.71 to 59.62, 0.9824)	53.30 (48.90 to 58.06, 0.9824)	52.20 (47.88 to 57.84, 0.9824)
Aq	**96.60 (91.62 to 101.99, 0.9979)**	**96.20 (91.39 to 101.76, 0.9979)**	**91.20 (86.65 to 96.64, 0.9979)**
DCM-ALK	**85.80 (80.49 to 90.98, 0.9851)**	**85.31 (80.17 to 90.86, 0.9851)**	**84.70 (79.82 to 89.06, 0.9851)**

(*): Actinomycin D (CC_{50}=nM)

Table 2. IC_{50s} of the inhibition of NF-κB production, calculated for the extracts from *D. draco*. IC_{50} was calculated using Prism v8.4.0 (GraphPad Software) using non-linear regression, dose-response curves. CI95%: Confidence interval 95%/Tukey's multiple comparisons test (p<0.001***).

Extracts	Inhibition of NF-κB production (IC_{50} μg/mL) at 48 h (CI95%, R2)		
	THP-1	HaCaT	NIH-3T3
Untreated cells	19.98 (14.41 to 24.78, 0.9886)	17.24 (12.92 to 22.61, 0.9886)	16.46 (11.36 to 21.13, 0.9886)
Celastrol*	7.44 (2.72 to 11.33, 0.9891)	7.41 (2.43 to 12.90, 0.9891)	7.40 (2.76 to 12.40, 0.9891)
HEX	85.61 (80.27 to 90.72, 0.9568)	**83.94** (78.13 to 88.77, 0.9568)	**81.81** (76.24 to 86.93, 0.9568)
DCM	**60.80 (55.13 to 65.11, 0.9856)**	**60.52 (55.73 to 65.61, 0.9856)**	**58.90 (53.95 to 63.95, 0.9856)**
MeOH	49.93 (44.40 to 54.63, 0.9512)	46.33 (41.53 to 51.99, 0.9512)	46.26 (41.32 to 51.43, 0.9512)
Aq	93.79 (88.85 to 98.84, 0.9615)	93.71 (88.72 to 98.22, 0.9979)	91.35 (86.43 to 96.53, 0.9979)
DCM-ALK	**65.69 (60.19 to 70.40, 0.9863)**	**65.06 (60.28 to 70.82, 0.9863)**	**64.10 (59.93 to 69.73, 0.9863)**

(*): Celastrol (IC_{50}=μM)

Table 3. EC_{50s} of the activation of Nrf2 production, calculated for the extracts from *D. draco*. EC_{50} was calculated using Prism v8.4.0 (GraphPad Software) using non-linear regression, dose-response curves. CI95%: Confidence interval 95%/Tukey's multiple comparisons test (p<0.001***).

Extracts	Activation of Nrf2 production (EC_{50} μg/mL) at 48 h (CI95%, R2)		
	THP-1	HaCaT	NIH-3T3
Untreated cells	1.96 (-4.54 to 6.52, 0.9973)	1.95 (-4.73 to 6.12, 0.9973)	1.89 (-4.43 to 6.94, 0.9973)
CDDO-Me*	0.11 (0.06 to 0.16, 0.9953)	0.11 (0.06 to 0.16, 0.9953)	0.10 (0.05 to 0.15, 0.9953)
HEX	57.01 (52.52 to 62.40, 0.9609)	56.41 (51.77 to 61.18, 0.9609)	53.98 (48.63 to 58.38, 0.9609)
DCM	**24.75 (19.90 to 29.85, 0.9987)**	**22.53 (17.38 to 27.27, 0.9987)**	**22.12 (17.98 to 27.68, 0.9987)**
MeOH	17.69 (12.49 to 22.48, 0.9781)	12.94 (7.90 to 17.81, 0.9781)	10.47 (5.28 to 15.09, 0.9781)
Aq	68.82 (63.93 to 73.24, 0.9873)	67.65 (62.06 to 72.85, 0.9873)	63.70 (58.14 to 68.89, 0.9873)
DCM-ALK	**28.95 (23.44 to 33.61, 0.9968)**	**26.58 (21.53 to 31.77, 0.9968)**	**25.84 (20.50 to 30.71, 0.9968)**

(*): CDDO-Me (IC_{50}=nM)

Table 4. *In vitro* culture plates (agar cup plate method) of *D. draco* extracts showing the zone of inhibition (ZI) concentration against different strains of microorganisms. IC_{50s} of the ZI was calculated using Prism v8.4.0 (GraphPad Software) using non-linear regression, dose-response curves. CI95%: Confidence interval 95%/Tukey's multiple comparisons test (p<0.001***).

Extracts	Zone of inhibition at (IC_{50} μg/mL) at 48 h (CI95%, R2)		
	S. aureus	*E. coli*	*C. albicans*
Ofloxacin*	27.65 (22.37 to 32.11, 0.9941)	27.67 (22.28 to 32.09, 0.9941)	27.71 (22.28 to 32.94, 0.9941)
HEX	93.56 (88.02 to 98.56, 0.9816)	94.19 (89.11 to 99.98, 0.9816)	96.39 (91.99 to 101.40, 0.9816)
DCM	**27.19 (22.69 to 32.34, 0.9925)**	**27.41 (22.63 to 32.35, 0.9925)**	**29.37 (24.38 to 34.87, 0.9925)**
MeOH	54.67 (49.53 to 59.51, 0.9847)	55.61 (50.38 to 60.42, 0.9847)	56.22 (51.75 to 61.32, 0.9847)
Aq	89.92 (84.84 to 94.45, 0.9869)	86.78 (81.08 to 91.34, 0.9869)	88.14 (83.70 to 93.65, 0.9869)
DCM-ALK	**21.23 (16.51 to 26.65, 0.9928)**	**22.57 (17.90 to 27.97, 0.9928)**	**24.47 (19.58 to 29.30, 0.9928)**

(*): Ofloxacin (IC_{50}=μM)

Table 5. Minimum inhibitory concentration (MIC) of *D. draco* extracts against different strains of microorganisms. MIC was calculated using Prism v8.4.0 (GraphPad Software) using non-linear regression, dose-response curves. CI95%: Confidence interval 95%/Tukey's multiple comparisons test (p<0.001***).

Extracts	Minimum inhibitory concentration at (MIC μg/mL) at 48 h (CI95%, R2)		
	S. aureus	***E. coli***	***C. albicans***
Ofloxacin*	27.65 (22.48 to 32.28, **0.9992**)	27.67 (22.28 to 32.85, **0.9992**)	27.71 (22.91 to 32.83, **0.9992**)
HEX	87.33 (82.22 to 92.39, 0.9958)	89.71 (84.78 to 94.68, 0.9958)	91.24 (86.05 to 96.18, 0.9958)
DCM	**24.04 (19.99 to 29.30, 0.9927)**	**25.49 (20.24 to 30.66, 0.9927)**	**26.75 (21.46 to 31.56, 0.9927)**
MeOH	48.78 (43.57 to 53.85, 0.9908)	52.85 (47.72 to 57.07, 0.9908)	53.88 (48.52 to 58.80, 0.9908)
Aq	81.64 (76.99 to 86.25, 0.9944)	83.62 (78.82 to 88.04, 0.9944)	86.36 (81.84 to 91.73, 0.9944)
DCM-ALK	**18.58 (13.92 to 23.39, 0.9924)**	**19.42 (14.05 to 24.05, 0.9924)**	**19.92 (14.61 to 24.32, 0.9924)**

(*): Ofloxacin (IC_{50}=μM)

Table 6. CC_{50s} of the LDH (cytotoxicity) assays calculated for the compounds from *D. draco*. CC_{50} was calculated using Prism v8.4.0 (GraphPad Software) using non-linear regression, dose-response curves. CI95%: Confidence interval 95%/Tukey's multiple comparisons test (p<0.001).

Samples	Cytotoxicity (CC_{50} μM) at 48 h (CI95%, R2)		
	THP-1	**HaCaT**	**NIH-3T3**
Untreated cells	99.78 (94.11 to 104.60, 0.9807)	98.96 (93.39 to 103.83, 0.9807)	98.98 (93.75 to 103.71, 0.9807)
DMSO	20.34 (15.23 to 25.45, 0.9819)	20.34 (15.70 to 24.62, 0.9819)	20.12 (15.18 to 25.59, 0.9819)
Actinomycin D*	7.96 (2.76 to 12.43, 0.9924)	7.95 (2.56 to 11.94, 0.9924)	7.95 (2.28 to 12.04, 0.9924)
Compound 1	87.95 (82.04 to 92.15, 0.9913)	87.61(82.66 to 92.79, 0.9913)	87.12 (82.85 to 92.11, 0.9913)
Compound 2	69.31 (64.31 to 74.49, 0.9958)	67.55 (62.06 to 72.84, 0.9958)	66.77 (61.25 to 71.61, 0.9958)
Compound 3	75.41 (70.44 to 80.12, 0.9951)	74.27 (69.57 to 79.22, 0.9951)	71.58 (66.07 to 76.35, 0.9951)

(*): Actinomycin D (CC_{50}=nM)